Preferential solvation of Ca^{2+} in aqueous solutions containing ammonia: A molecular dynamics study

Cite as: J. Chem. Phys. **116**, 5460 (2002); https://doi.org/10.1063/1.1453957
Submitted: 16 July 2001 • Accepted: 07 January 2002 • Published Online: 19 March 2002

F. M. Floris, José M. Martínez and J. Tomasi

Preferential solvation of Ca^{2+} in aqueous solutions containing ammonia: A molecular dynamics study

F. M. Floris, José M. Martínez,[a] and J. Tomasi
Dipartimento di Chimica e Chimica Industriale, Universitá di Pisa, Via Risorgimento 35, 56126 Pisa, Italy

(Received 16 July 2001; accepted 7 January 2002)

Ca^{2+} aqueous solutions containing different proportions of ammonia have been studied by means of molecular dynamics simulations. Previously developed *ab initio* effective pair potentials, in the framework of the polarizable continuum model, and only tested at a cluster computation level, have been employed to describe ion–ligand interactions. Structural and dynamic changes present in the neighborhood of the ion as a function of the ammonia concentration have been followed. Results show a preferential solvation for ammonia, even at very low concentrations. For the pure aqueous solution, calcium ion is coordinated by eight water molecules, while the presence of ammonia favors an equilibrium between an octa and enna-coordinated situation when this ligand becomes predominant, confirming the prediction of cluster calculations. However, the increase in the coordination number is followed by an intrinsic loss of stability for the identifiable solvated structures because of the larger tendency of ammonia to participate in solvent exchange phenomena. Solvent exchange events show, for the most simple case (water–water exchange), a marked mechanistic variety. © *2002 American Institute of Physics.* [DOI: 10.1063/1.1453957]

I. INTRODUCTION

Nowadays, empirical or theory based ion–water interaction potentials are available for many different cations, from alkaline to lanthanides. One of the cations that has merited much interest is Ca^{2+}. From a biological point of view, the importance of calcium ion is beyond question. Among other features, this ion is involved in the structure and functionality of metallo-enzymes, has an active role as an electrolytic message carrier or is used to maintain the osmotic pressure in the cells by means of the pumps working across the cell membrane.[1–3] A proper understanding of all the processes Ca^{2+} is involved in, implies a deep knowledge of its solvation features. Most of the statistical simulations performed so far and dealing with the solvation phenomenon of this cation are specifically devoted to the study of the hydration[4–18] of calcium ion, and, marginally, solvation properties including other solvents have been considered at a quantum chemical level.[19–23] To our best knowledge, only the work done by Sidhisoradej *et al.*[24] studies the solvation of Ca^{2+} in liquid ammonia by means of molecular dynamics (MD) simulations using a potential function which explicitly considers three-body effects in the ion–solvent potential. However, studies including more than one solvent have not been considered so far, despite being the most common situation in the biological media. The work presented here supposes the natural extension of the preceding work[25] in which calcium–water and calcium–ammonia *ab initio* effective pair potentials were developed to account for such situations. The polarizable continuum model was employed, for the first time in a multicomponent medium, to take into account the many-body effects present in the ion neighborhood. Structural and energetic analysis was done for a set of clusters accounting for different coordination situations. Now, a set of MD simulations, using those potentials, are presented for aqueous solutions containing small quantities of ammonia, focusing our attention on structural and dynamic aspects.

II. MOLECULAR DYNAMICS SIMULATIONS

Molecular dynamics simulations were performed in the microcanonical ensemble (*NVE*) using cubic cells with periodic boundary conditions. Different simulations containing a Ca^{2+} ion with 400 solvent molecules were performed, the difference among them being the ammonia/water proportion. In this way, the influence of the solvent composition in the set of properties considered has been studied. Calcium–water and calcium–ammonia potentials developed in the previous work[25] are used to describe ion–solvent interactions. Water was modeled by the SPC/E model[26] and ammonia by means of the recent OPLS type of potential of Rizzo and Jorgensen.[27] Lorentz–Berthelot rules are applied to describe water–ammonia interactions. Table I labels and summarizes the set of performed simulations. In all cases the box side (L) was 22.924 Å, yielding densities in the range 0.995–0.998 g/cm^3. All systems were equilibrated at 298 K for 50 ps before the production period. In order to be coherent with the use of the water dielectric constant in the development of the cation–solvent interaction potentials as detailed in Ref. 25, the ammonia/water ratio in the simulation box was maintained low enough. This low content of ammonia can create convergence problems if these molecules are randomly distributed in the simulation cell: the probability of interacting with the ion could be too low to be observed in a reasonable time (<1 ns). In order to reduce this potential problem, ammonia molecules were located in the neighborhood of the metal ion. In this way, during the equilibration period the

[a]On leave from Departamento de Química Física, Universidad de Sevilla, 41012-Sevilla, Spain, electronic mail: josema@simulux.us.es

TABLE I. Summary of the performed simulations.

Simulation code	System composition	R_0[a] (Å)	Free dynamics (ps)	Analysis (ps)
A	$Ca^{2+}+400\ H_2O$	⋯	500	500
B	$Ca^{2+}+399\ H_2O+1\ NH_3$	4.75	750	Last 500
C_1	$Ca^{2+}+392\ H_2O+8\ NH_3$	2.65	1000	Last 500
C_2	$Ca^{2+}+392\ H_2O+8\ NH_3$	4.75	1000	Last 500
D	$Ca^{2+}+380\ H_2O+20\ NH_3$	2.65[b] 4.75[c]	750	Last 500

[a]Ca–N distance used in expression (1) during the equilibration period.
[b]Eight ammonia molecules were constrained during equilibration to the harmonic potential at this R_0 value.
[c]Twelve ammonia molecules were constrained during equilibration to the harmonic potential at this R_0 value.

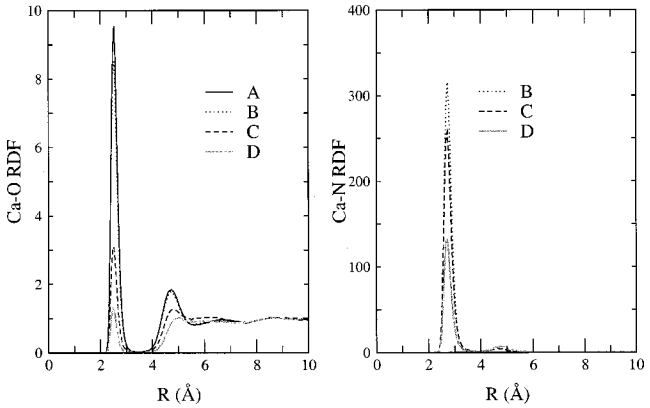

FIG. 1. Ca–O and Ca–N radial distribution functions.

dynamics of NH_3 molecules was constrained by an *extra* harmonic potential, V_{harm}, that defines an effective range for the Ca–N distance:

$$V_{\text{harm}}=K(R_{\text{Ca–N}}-R_0)^2. \tag{1}$$

The harmonic constraint was switched off at the end of the equilibration period allowing molecules to follow normal dynamics. A value of K equal to 10 kcal/(mol Å^2) was enough to maintain ammonia molecules in the desired range (first or second solvation shell regions) without observing any shifting in the temperature after removing the constraint. Table I also collects the values of R_0 used during the equilibration period in each case. The production period for each simulation was determined then as a function of the evolution of the systems after removing V_{harm}. This evolution was followed structurally by means of the Ca–O and Ca–N radial distribution functions. Typically, some hundreds of picoseconds were needed before convergence in the radial distribution functions (RDFs) (Table I).

In the case of the simulation containing eight ammonia molecules, two simulations (C_1 and C_2) were done, the difference being just the position of the ammonia molecules during the equilibration period. In simulation C_1, these were located in the first solvation shell, while in the second case, they were constrained to remain in the second shell. After a half nanosecond of free dynamics, both simulations showed Ca–O and Ca–N distributions close enough to be considered equivalents and, moreover, they remained stable during the next 500 ps. For this reason, results concerning the system composed of one calcium ion, 392 waters, and 8 ammonia molecules will be the average obtained from simulations C_1 and C_2. In the case of simulation D, the initial situation for the free dynamics was that in which eight molecules of ammonia were located in the first solvation shell and the remaining twelve were positioned in the second.

All MD simulations were run with a modified version of the MOLDY program[28] that implements a symplectic integration algorithm of the leap-frog type to integrate equations of motion. Orientations of solvent molecules, which were assumed to be rigid, were described by the quaternion formalism.[29] The time step was set up to 2 fs, and Coulombic interactions computed by the Ewald sum technique.[30] A spherical molecular cutoff of $L/2$ was applied to the real space part of the Ewald energy as well as to the short range contributions.

The evolution of the properties with the system composition will be considered at three different levels regarding the structure, dynamics, and solvent exchange phenomena in the solutions considered.

III. RESULTS AND DISCUSSION

A. Structure

1. RDFs and coordination numbers

RDFs obtained in each simulation for the Ca–O and Ca–N pairs are plotted in Fig. 1 while Table II collects the positions of maxima of each distribution and the corresponding integration numbers, including individual contributions of each solvent, for each shell. In all cases, well-defined first solvation shells are observed from both Ca–O and Ca–N distributions.

Results from simulation A, which constitutes our reference, define a first hydration shell containing eight water

TABLE II. Ca–O and Ca–N RDF maxima positions (Å) and integration numbers.

	First shell					Second shell				
	RDF maximum		Integration number			RDF maximum		Integration number		
Simulation	Ca–O	Ca–N	H_2O	NH_3	Total	Ca–O	Ca–N	H_2O	NH_3	Total
A	2.51	⋯	8.01	⋯	8.01	4.71	⋯	17.4	⋯	17.4
B	2.51	2.72	7.12	0.86	7.98	4.71	4.50	16.9	0.1	17.0
C	2.49	2.70	2.55	5.90	8.45	4.80	4.65	13.5	0.8	14.3
D	2.47	2.69	1.00	7.70	8.70	5.0	4.71	10.4	3.3	13.7

molecules at a mean distance of 2.51 Å. A quite less defined second hydration shell is centered around 4.7 Å containing almost 17.5 water molecules, providing a picture in which each water molecule of the first shell interacts with approximately two water molecules of the second one via two hydrogen bondings.

Experimentally, techniques such as x-ray diffraction (XRD),[4,31,32] neutron diffraction (ND),[33] or extended x-ray absorption fine structure (EXAFS), and large angle x-ray scattering (LAXS),[17] spectrocopies have provided a wide range of values for the most probable mean distance (2.33–2.49 Å) and number (6–10) of molecules in the first hydration shell.[34] Facts like the dependence of the coordination number with the salt concentration are not clearly stated yet, and results depend on the experimental technique.[35] Previous statistical mechanics simulations dealing with the Ca^{2+} hydration[4–18] also offer a nonunique picture of the hydration structure around the calcium ion. In particular, the previous calcium–water potential developed using the PCM methodology,[9] defined a first hydration shell centered at the same distance as the one here obtained but with a coordination number slightly larger, 8.6, which came from the equilibrium between structures containing eight and nine water molecules around the ion. Both potentials present the minimum of the ion–water interaction at the same distance but differ in 4.9 kcal/mol in the depth of the potential well (−47.7 vs −42.8 kcal/mol), the new potential being less attractive. This fact shows how slight differences in the interaction potentials may produce non-negligible differences in coordination numbers when energy differences between different plausible structures are low, as is the case of the Ca^{2+} ion.[25]

The most recent experimental[17] results propose eight as the most probable coordination number with a broad and asymmetric distribution of Ca–O distances centered at 2.46 Å. MD simulations based on a combined quantum mechanics/molecular mechanics strategy[13] find a coordination number of 8.3 with a mean distance of 2.45 Å, and show the dependence of the results on the accuracy of the quantum mechanically described part of the system as well. Our results agree with this picture of eight water molecules in the first shell, although the mean Ca–O distance is slightly longer. Experimental evidence of a less defined second hydration shell, centered at ~4.6 Å, has been pointed out by XRD[31] and LAXS[17] measurements. Our Ca–O RDF shown in Fig. 1 reveals, as already pointed out, the presence of this second maximum.

The introduction of ammonia in the solution progressively reduces the position of the first maximum in the Ca–O distribution, and has the opposite effect on the peak defining the second hydration shell. However, from system A to system D, the displacements are quite different in magnitude, −0.04 and +0.29 Å for the first and second maxima, respectively. In addition, the presence of ammonia clearly reduces the definition of the second water shell, which practically disappears in the simulation with the highest content of ammonia. The evolution of the maxima in the Ca–N RDFs with the ammonia concentration is the same as that found for water.

Positions of the first maximum in both Ca–O (simulation A) and Ca–N (simulation D) distributions are roughly 0.05 Å shorter than the distances found when optimizing the $[Ca(H_2O)_8]^{2+}$ and $[Ca(NH_3)_8]^{2+}$ clusters using the effective pair potentials.[25] This shrinkage of the solvated ion, due to the effects of the condensed medium, is markedly larger than that observed in cations with the same charge but with a more tightly bound first hydration shell.[36]

Composition of the first two solvation shells is clearly altered with the presence of ammonia (Table II). Interestingly, not only the composition of each shell is changed, but also the total number of molecules found in each region. In this sense, opposing effects are observed in each sphere when increasing the quantity of ammonia present in the solution: while the first solvation shell increases from 8 to 8.7, the second decreases from 17.4 to 13.7. In both shells, the number of water molecules is reduced when going from simulation A to D, while the content of ammonia follows the opposite trend. In simulation B, the single ammonia molecule present in the solution spends 86% of the time in the first shell, replacing one of the water molecules, and the remaining 14% in the second, not leading to marked differences with respect to simulation A. For simulation C, almost six of the eight ammonia remain in the first shell, and in the case of simulation D, this figure is increased up to 7.7. Therefore, a preferential solvation in the coordination sphere of Ca^{2+} ion is observed, favoring the presence of ammonia in the neighborhood of the ion, even at concentrations as low as the ones used here.

The analysis of the first shell coordination number distribution (Fig. 2) as a function of the ammonia content shows that, in simulations A and B, the situation with eight molecules in the first shell is almost the only one present. However, when the ammonia concentration is increased a shift to coordination number equals nine is observed, becoming the most probable situation in the case of simulation D. The marked decrease in the number of molecules defining the second shell, from 17.4 to 13.7, can be understood on the basis of two facts. On the one hand, the presence of ammonia molecules in the second shell may disrupt the water structure present in the infinitely diluted aqueous solution of Ca^{2+}. On the other hand, the lower ability of the ammonia molecule to donate its hydrogen atoms to form hydrogen bonds between the first and the second shells reduces the *ability* of the first shell to fix molecules of the second, reaching a value of 1.6 for the ratio second/first coordination numbers. This value has to be compared with 2.2, the value obtained in pure water. This explanation should not be identified with the absence of specific binding sites (hydrogen atoms) in the first shell. These are present when the first solvation shell is mainly composed of ammonia as well, but the energetics associated with the interactions in such bindings points is different. As previously shown,[37] the absence of such specific binding sites for the first–second shell interactions leads to a marked increase in the coordination number associated with the second solvation shell. The orientation of water molecules is in that case very different from what is found in simulations containing an explicitly defined ion first solvation shell (see Sec. III A 2).

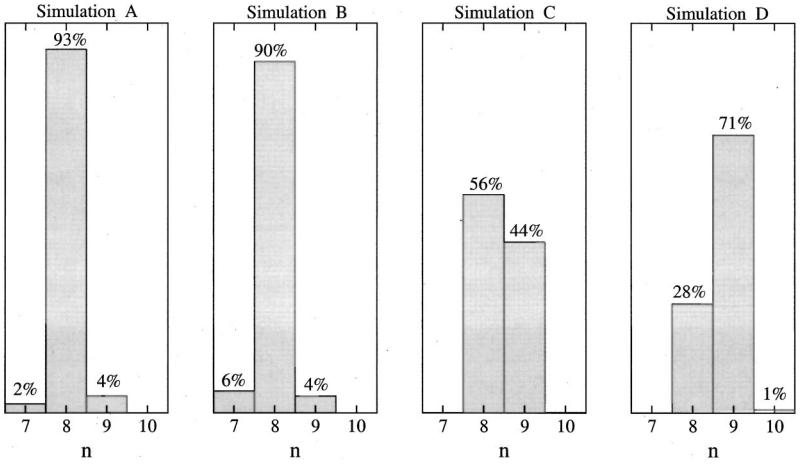

FIG. 2. Coordination number distributions.

2. First shell structure

Figure 3 shows the orientation of the solvent molecules as a function of the metal–solvent distance, defined by the orientational parameter (θ), i.e., the angle formed by the Ca–X (X=N,O) vector and that defining the dipole moment of water or ammonia. For water molecules in the first shell the mean value of θ is 161° in simulations A and B, while this figure is increased up to 170° in the case of ammonia (B, C, and D simulations).

Experimentally, this out-of-planarity for the metal–water arrangement is found by means of neutron diffraction measurements, which report a value of $145° \pm 9°$ for a concentrated aqueous solution of $CaCl_2$.[33] The theoretical value predicted for a pure ion–dipole interaction, and found in previous cluster calculations,[25] is 180°. However, the thermal energy and the solvent–solvent interactions promote the appearance of this tilt angle, more pronouncedly in the water case. This effect is more prominent in the second solvation shell in which this parameter lowers down to 120° for water molecules while in the case of ammonia a mean value around 160° is found. These results give an indication of the balance between the two types of interactions (ion–solvent and solvent–solvent), showing the dominant contribution in each case, even at relatively large distances (~5 Å). As long as the number of ammonia molecules in the first and second solvation shells increases, the relative role of the solvent–solvent interaction is reduced, and the value of θ for water molecules in the first–second shell region is shifted to higher values, as a consequence of the radial orientation imposed by the ion (see Figure 3).

The last structural parameter analyzed is the X–Ca–X′ (X,X′=O,N) angle distribution. It provides information about the possible coordination polyhedra adopted by the first shell solvent molecules. Figure 4 shows the distributions obtained for the four simulations, regardless of the pair of molecules involved. Simulations A and B provide exactly the same distribution, while in simulations C and D the two well-defined maxima present in all cases are shifted to lower values. This displacement is the consequence of the increasing weight of structures containing nine molecules in the first shell.

This effect is clearly shown in Fig. 5(a) in which contributions coming from structures with eight and nine solvent molecules in the first shell are plotted for simulations C and D. The two maxima are centered at 74° and 141° for solvation shells with eight molecules, and at 71° and 137° for the cases with nine molecules. Figure 5(a) also reports the discrete distribution of values obtained when considering two different regular polyhedra: square antiprism, with eight vertices, and tricapped trigonal prism, with nine vertices. In the

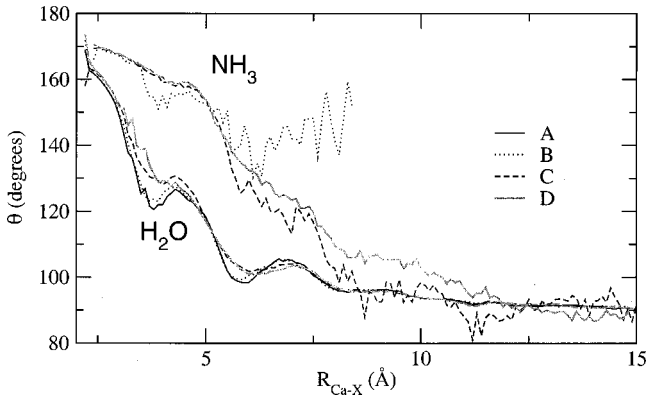

FIG. 3. Mean value of the angle θ, formed by the Ca–X (X=O,N) and solvent dipole vectors, as a function of the ion–solvent distance.

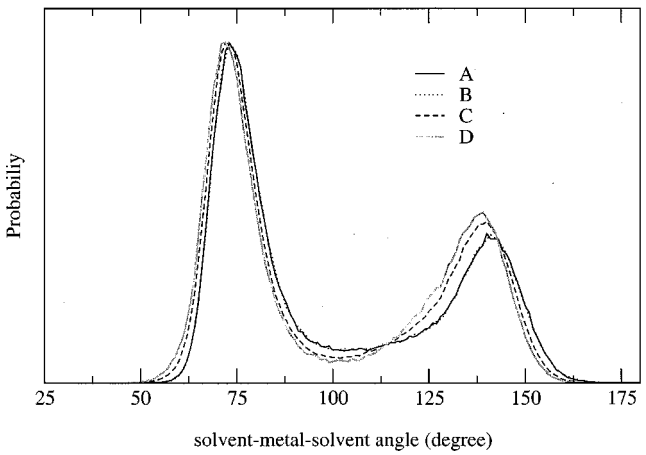

FIG. 4. First shell solvent–metal–solvent angle distributions for simulations A–D.

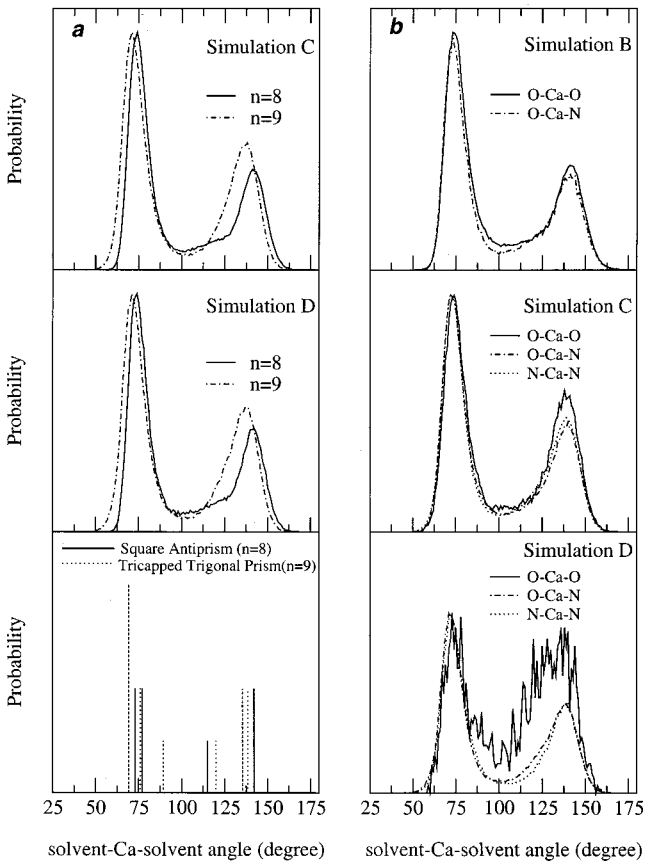

FIG. 5. (a) Angle distributions obtained for structures with eight and nine solvent molecules in the first coordination sphere in simulations C and D. The botton panel shows the discrete histogram obtained for the square antiprism and tricapped trigonal prism, compatible with the previous distributions. (b) Contributions of the three different possible solvent pairs to the angle distribution of Fig. 4 (simulations B–D).

case of the square antiprism, when some (thermal) disorder is included, the two maxima appearing at 73° and 77° should define a broader peak centered at ~74°–75° with roughly double intensity compared to that observed at ~142°. This is, in fact, the image supported by the angular distributions provided by the simulations, and in agreement with previous results.[13,38]

Interestingly, the presence of the two solvents, and in different proportions in the first shell, does not alter the average structure. In the case of nine-coordinated distributions, in addition to the shifting of the two maxima to lower values, a clear increase in the intensity of the distributions in the region between 120° and 145° is observed. The distribution of angles observed in the tricapped trigonal prism is in agreement with this shifting of the maxima to lower values as well; taking into account the relative intensities, both maxima should appear around 72° and 137°, and a decrease in the first/second maxima intensities ratio should also be observed. Although differences between both theoretical structures are small (displacements on the order of 3°–4°), distributions obtained for each coordination number strictly follow the predicted changes. Therefore, both regular structures can be considered as representative ones for the two situations.

An interesting feature, only available when more than one type of ligand is present in the coordination sphere, is the the contribution of each pair of ligands. Figure 5(b) shows the contributions obtained in simulations B, C, and D for the three possible pairs, i.e., water–water, ammonia–ammonia, and water–ammonia. Such distributions are remarkably similar in all cases; the only exception is given by the water–Ca–water distribution of simulation D where there is a large noise due to the very low probability of finding two water molecules in the first solvation shell (Table II). The only appreciable difference is the slight preference of water molecules to occupy relative positions with large water–Ca–water angles. This can be explained by looking at the ordering of repulsive energies of ligand pairs in the first solvation shell. Cluster computations of the type presented in the preceding paper[25] show that repulsive interactions between molecules in the first solvation shell decrease in the order water–water>water–ammonia>ammonia–ammonia. Nonetheless, differences are very small, and no specific arrangements for the relative distribution of the different solvent molecules in the solvation sphere of the ion can be inferred.

TABLE III. Self-diffusion coefficient of Ca^{2+}, computed from the mean-square-displacement (MSD) and velocity autocorrelation function (VACF). Values in 10^{-5} cm^2 s^{-1}. Statistical uncertainties are ~7%–10%.

Simulation	MSD	VACF
A	0.52	0.52
B	0.68	0.68
C	0.61	0.60
D	0.67	0.71

B. Dynamics

1. Translational and librational motions

Mobility of the calcium ion in terms of the self-diffusion coefficient ($D_{Ca^{2+}}$) in the different simulations have been estimated from the slope of the ionic mean square displacement and from the integration of the velocity autocorrelation function (VACF).[30] Results are shown in Table III. Both approaches provide the same results, whose differences, when present, are below the statistical uncertainties. The replacement of water by ammonia in the first hydration shells increases by 16%–35% the mobility of the calcium ion but without a clear pattern for the evolution of $D_{Ca^{2+}}$ with the ammonia content. The available experimental value for $D_{Ca^{2+}}$ in water is 0.79×10^{-5} cm^2 s^{-1}, so in our case (simulation A) the mobility of the ion is underestimated. This fact has been previously observed in other calcium–water potentials,[7,15,18] either with an empirical or quantum mechanical origin.

The power spectra for the calcium ion and the first shell solvent molecules have been computed by means of the Fourier transform of the center of mass VACF and displayed in Fig. 6. The spectral densities obtained for the metal ion in the different simulations are characterized by the presence of three maxima in all cases. The first one, located at ~30 cm^{-1} is independent of the solution composition. However, this is not the case for the second (~150–160 cm^{-1}) and particu-

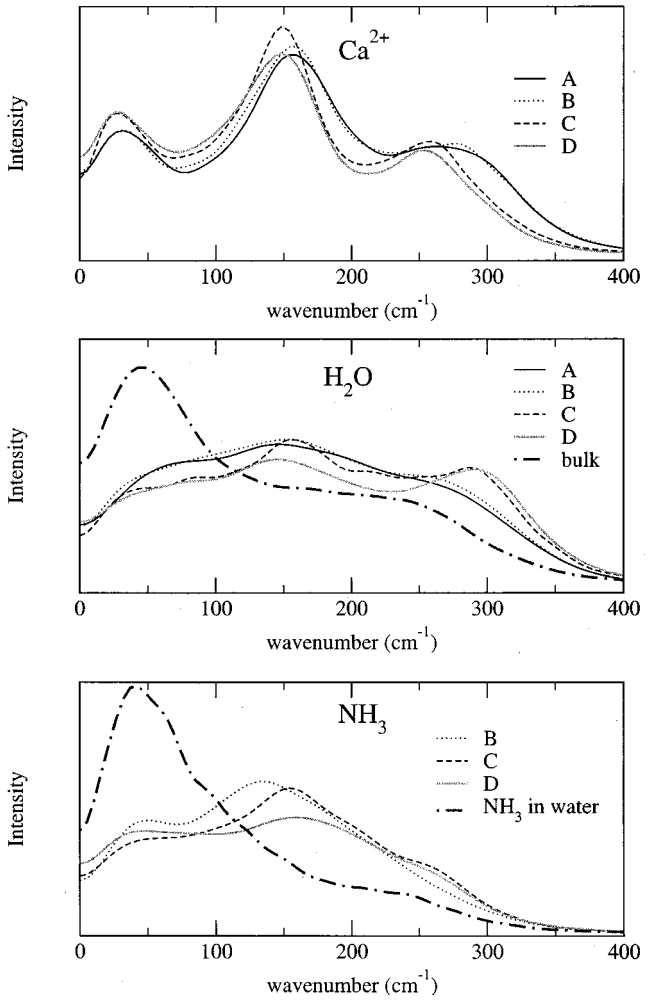

FIG. 6. Fourier transforms of the velocity autocorrelation functions of the calcium ion and the first shell water and ammonia molecules for simulations A–D. Spectra of pure water (bulk) and highly dilute ammonia aqueous solution (NH_3 in water) are shown as well.

larly the third ($\sim$250–280 cm^{-1}) maximum, that evolve to lower values when the ammonia content is increased, in correspondence with the tendency observed in the VACFs. Spectra obtained for the first shell solvent molecules, although quite less structured, show similar maxima as well, sometimes transformed into simple shoulders. The spectrum corresponding to a pure water solution and a highly dilute solution of ammonia in water are included as well. In both cases clear differences between the reference spectra (water in water and ammonia in water) and those obtained in the different solutions containing the ion are observed. The evolution of the spectra with the ammonia content shows in the case of water a better definition of the third maximum appearing at $\sim$300 cm^{-1}. For ammonia, a similar behavior is found, although in this case the maximum is transformed into a shoulder around 250 cm^{-1}. By means of Raman measurements, symmetric metal–solvent stretching vibrations can be determined when the interaction between the metal ion and its coordinated solvent molecules is strong enough. For a Ca^{2+} aqueous solution, a value of 290 cm^{-1} was found,[39] while in the case of an ammonia solution containing this ion, that figure was reduced to 260–266 cm^{-1}.[40] A projection of the instantaneous center of mass velocity along the oxygen(nitrogen)–calcium direction was performed as well. The corresponding Fourier transforms of this projected VACF, provided as supplementary material,[41] show in all cases that the relative intensities of the maxima are changed, the region above $\sim$200 cm^{-1} showing higher relative intensities. In contrast to what was observed in previous MD simulations[36,42,43] with more rigid cation first hydration shells, even the projected velocities provide spectra with broad and not resolved maxima, probably due to a mix of frequencies associated with solvent intermolecular normal modes that appear at similar frequencies. This fact complicates the analysis and make conclusions less obvious. Nonetheless, for the water case, the indexing of the maximum of highest frequency with the metal–water vibration is coherent with the results of simulations C and D, in which the main component of the maximum located at $\sim$300 cm^{-1} is associated with the metal–oxygen vibration (projected VACF). In the case of ammonia, however, Fourier transforms of the projected VACFs do not define in a clear way the shoulder appearing at highest frequency.

2. Solvent reorientational motions

With the aim of analyzing the reorientational motion of solvent molecules in the first solvation sphere, a set of reorientational time correlation functions defined as

$$C_l^i(t) = \langle P_l(\mathbf{u}_i(0)\cdot\mathbf{u}_i(t))\rangle, \tag{2}$$

where P_l is the lth Legendre polynomial and $\mathbf{u}_i$ is a unit vector that characterizes the orientation of the molecule, have been calculated. $C_l(t)$ values are computed using a coordinate frame based on the molecule and the reorientational times by fitting the long time decay of the function to an exponential form.

In the case of water, a vector defining the dipole moment of the molecule (μ), the intramolecular proton–proton vector ($H-H$), and a third one perpendicular to the solvent plane ($\perp$) were used, while for ammonia, due to the higher internal symmetry (two moments of inertia are equal), only the component along the dipole moment and one perpendicular to that have been used (the third is equivalent to the latter). $C_l(t)$ functions with $l=1,2$ may be related to spectroscopic measurements[30,34] and results obtained for these two orders are shown in Table IV. For comparative purposes, MD reorientational times, using the same interaction potentials, for pure water and a dilute aqueous ammonia solution are included as well.

In the case of water, as previously found for other properties, simulations A and B provide the same results. The increase of ammonia content in the first and second solvation shells is followed by an increase of the different τ's computed for water, reflecting a slower rotational dynamics. Anyhow, the reorientational motion component associated with the dipole moment of the water molecule is the one highly hindered by the ion–water interaction, with respect to the bulk case: the ratios first-shell/bulk are in the range 6–8 for such component. This is just another way of visualizing the radial orientation imposed by the ion field, previously discussed in terms of the θ angle.

TABLE IV. Reorientational correlation times (ps).

	First shell H_2O						First shell NH_3			
Simulation	τ_1^{H-H}	τ_1^{μ}	$\tau_1^{\perp}$	τ_2^{H-H}	τ_2^{μ}	$\tau_2^{\perp}$	$\tau_1^{\perp}$	τ_1^{μ}	$\tau_2^{\perp}$	τ_2^{μ}
A	4.9	31.9	4.7	3.0	10.8	3.0	⋯	⋯	⋯	⋯
B	5.1	32.2	4.7	3.7	11.0	3.4	0.7	37.6	⋯	12.6
C	7.2	39.0	7.1	4.6	13.3	4.1	1.0	38.3	⋯	10.3
D	8.5	38.4	8.2	5.2	13.0	14.1	1.2	30.1	0.8	10.8
NH_3[a]							0.6	2.6	0.5	0.9
SPC/E[b]	4.8	5.0		2.6	2.2					

[a]Reorientational times for OPLS NH_3 (Ref. 27) in SPC/E water. See the text for details.
[b]Reorientational times for SPC/E pure water (Ref. 18).

In the case of ammonia, the $\perp$ component is just slightly higher than that obtained in a highly dilute solution of ammonia in water. However, the μ component presents reorientational times in all cases much larger than the reference values, even more than in the water case. Again, this is in agreement with the higher response observed by the ammonia solvent to the cation field (Fig. 3). The increase of the ammonia content in the solution, however, slightly reduces the computed τ's for the μ component.

The experimental information available regarding the rotational dynamics of the solvent comes from aqueous solutions nuclear magnetic resonance (NMR) relaxation data, that can be compared with the τ_2^{H-H} values. Chizhik[44] estimated the reorientational time of water in the first hydration shell of the calcium ion as the ratio between the value in the first shell and that found in the bulk, obtaining 3.3. Using the MD data of Table IV, that ratio reports 1.2, so, in principle, our potential underestimates such property. However, it is worth pointing out that in that work hydration numbers of 6 and 12 were supposed for the first two hydration shells of Ca^{2+} (to be compared with results of Table II) and that the experimental range of concentrations covered solutions one order of magnitude more concentrated than that of simulation A.

3. Lability of the solvation shells

One of the properties that can provide information about the lability of the solvation shells of a given ion is the mean residence time (MRT) of solvent molecules inside those shells. This quantity informs about the probability a given molecule has of remaining inside a given solvation sphere. Calculations have been carried out using the method of Impey *et al.*,[45] which is based on the definition of a function, $n_{ion}(t)$, which measures the number of molecules belonging to the considered region around the ion after a period of time *t*. Excluding an initial period for which the function decays rapidly, $n_{ion}(t)$ follows an exponential form, i.e., $n_{ion} \propto e^{-t/\tau}$, where τ represents a characteristic relaxation time of the persistence of the molecules in the considered region. τ is the quantity defined as the mean residence time.

MRTs for water and ammonia (Table V) in the first two solvation shells of calcium have been computed using $t^* = 0$ ps[46] and $t^* = 2$ ps.[45] This parameter defines the maximum transient period a molecule can leave the considered region without losing its ascription to it. Experimentally, only the upper limit, $\tau_{exp} < 100$ ps, of mean residence times of water molecules in the first hydration shell of Ca^{2+} has been determined by means of NMR measurements.[34] The range defined by our results obtained for the aqueous solution, simulation A, is in very good agreement with this finding. It is interesting to notice that Koneshan *et al.*[15] estimated a MRT of 700 ps for waters in the first hydration shell performing MD simulations of dilute aqueous solutions of Ca^{2+} using theory based potentials as well.

In contrast to what has been observed in the structural properties previously analyzed, there is no clear pattern in the evolution of the first shell water MRTs when increasing the ammonia content. However, the computed first shell ammonia MRTs are progressively reduced. The shifting to lower values is particularly clear when transient periods ($t^* = 2$ ps) are allowed. Values obtained for molecules in the second shell are almost insensible to the composition of the first solvation shell, ammonia having a larger tendency to remain in this shell for longer periods than water. These results seem to indicate that the evolution of this property with the water/ammonia ratio is complex and, possibly, related to the probabilities for the different first–second shell exchange phenomena.

Mean lifetimes (see Table VI) for the different coordination numbers identified in the first solvation shell supplies information about their lability. Lifetimes with $t^* = 2$ ps have also been computed, defining in this case the maximum period in which transient changes in the coordination number are allowed. Although there is no physical basis for this choice, it will be interesting to check the effects of allowing

TABLE V. Mean residence times of first solvent molecules (ps).

		First shell		Second shell	
Simulation	t^* (ps)	H_2O	NH_3	H_2O	NH_3
A	0	44	⋯	4	⋯
	2	132	⋯	11	⋯
B	0	55	44	4	⋯
	2	136	262	11	⋯
C	0	37	43	4	8
	2	80	165	10	21
D	0	50	30	5	13
	2	171	91	11	15

TABLE VI. Mean lifetimes of first shell coordination numbers (ps).

Simulation	t^* (ps)	Coordination number $n=7$	$n=8$	$n=9$	$n=10$
A	0	0.3	6.1	0.4	⋯
	2	1.2	472.	1.6	⋯
B	0	1.3	6.1	0.5	⋯
	2	1.9	75.8	1.7	⋯
C	0	⋯	3.9	1.7	⋯
	2	⋯	14.4	13.2	⋯
D	0	⋯	1.8	1.5	⋯
	2	⋯	5.6	34.9	1.2

transient situations. The analysis performed does not take into account the chemical composition of the first coordination sphere. In fact, except for simulation B, the representative possibilities for each coordination number are far from being unique. (See supplementary material[41] for the distribution of the first shell species found for simulations B, C, and D that provides a clear picture about the heterogeneity found in the first solvation shell of calcium ion for simulations with both solvents). For simulations A and B, Table VI shows that octa-coordinated structures present a lower lability than those enna-coordinated. However, the situation abruptly changes when more ammonia is added to the solution and a clear stabilization of situations with nine molecules is observed in the last two simulations. Particularly interesting are the results obtained for simulation D. With $t^*=0$ ps, the eight and nine coordinated situations show lifetimes rather similar, but when t^* is increased up to 2 ps, the mean lifetimes obtained are clearly different, and the image supported by Fig. 2 is recovered. These results provide interesting dynamic information for the solvation phenomenon of Ca^{2+}, showing that, if no transient situations are allowed, structures with a coordination number equal to eight are always the most stable ones. Lastly, in spite of the large lifetimes obtained for the eight coordinated situations in simulation A, it should not be identified with a kind of rigidity in the internal arrangement of solvent molecules inside the solvation sphere. Figure 7 plots the evolution of all the first shell oxygen–calcium–oxygen angles observed for a 30 ps period of simulation A, in which no change in the hydration number was observed. The redistribution of solvent molecules is constant, even in relatively long periods without any solvent exchange or transient excursions to other solvation numbers. On the right-hand side of Fig. 7, angle distribution of simulation A (Fig. 4) is included as well for comparative purposes. Although cluster calculations[25] predicted as the most stable structure the square antiprism arrangement for an octa-coordinated calcium ion, in agreement with the average picture found in Fig. 4, no additional information was supplied regarding the facility this structure could be distorted. This type of information is difficult to obtain by such computations in which the dynamic picture of the minimized structure is lost. However, MD simulations can recover such type of information.

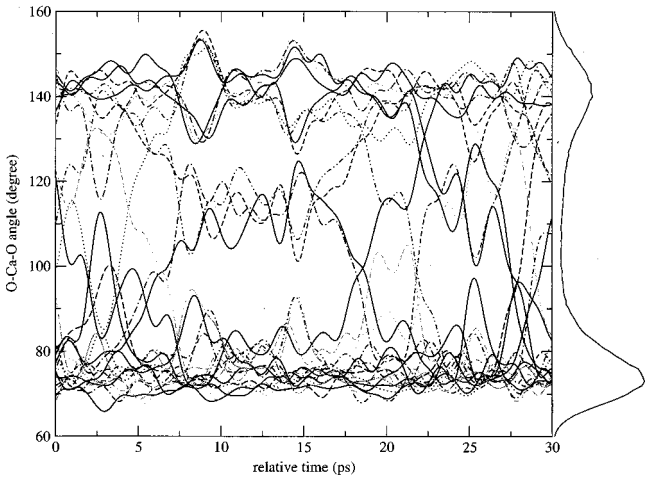

FIG. 7. Evolution of all the first shell oxygen–calcium–oxygen angles in a 30 ps period of simulation A in which no water exchange was found. The distribution of Fig. 4 is shown on the right-hand side.

C. Solvent exchange

From an experimental point of view, the kinetic characterization of simple ligand exchange around Ca^{2+} supposes a major challenge because of the high lability present in the first coordination shell for solvents like water.[47] Interestingly, this fact represents an advantage when a theoretical approach is followed, making the MD technique a useful tool to provide a microscopic information of the exchange phenomenon, as has been previously proved for other metal ions.[48,49] In the case of the aqueous solution, the simplest ligand substitution can take place, i.e., the exchange of one water molecule of the first shell by another of the second one:

$$[Ca(H_2O)_n]^{2+} + H_2O^* \rightleftharpoons [Ca(H_2O)_{n-1}H_2O^*]^{2+} + H_2O. \tag{3}$$

Using the distributions obtained in Fig. 2, it is clear that in the above-mentioned equilibrium, n is equal to 8. In fact, all transitions between the first two shells were identified by couples of water molecules that exchanged their ascription to one of the shells. From a general point of view (ligand substitution reactions[47,50]), substitutions can take place by a dissociative mechanism (through an intermediate with a reduced coordination number), by an associative mechanism (the intermediate presents a higher coordination number), or by an interchange process (there is no kinetically detectable intermediate). For the interchange mechanism a further distinction is made between associative (I_A) and dissociative (I_D) activation modes, depending on the strength of the ion-leaving/entering water interaction in the transition state structure.

The interchange mechanism seems to be the most probable one for relatively fast solvent exchange reactions (see Ref. 34, and references therein). The experimental detection of intermediates remains as a major challenge and the classification of the solvent exchange mechanisms is done in an indirect way, taking advantage of the sensitivity of the reaction rates to chemical or physical conditions.[50,51] In order to use MD simulations on this point, a criterion must established. The structural information provided by the radial dis-

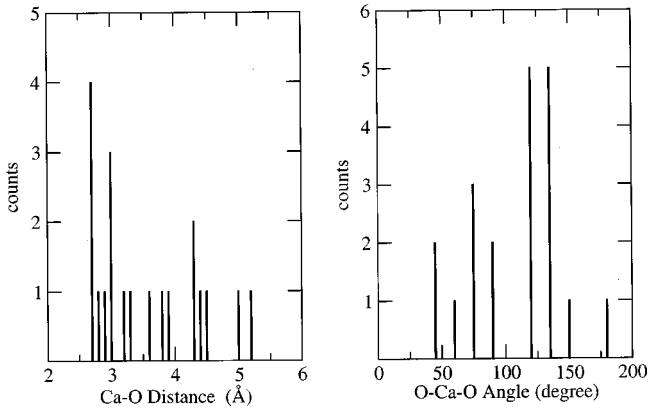

FIG. 8. Distributions of the Ca–O distances and O–Ca–O angles for the incoming and leaving water molecules around the moment of an exchange event in simulation A.

tribution functions of Fig. 1 may be used for that purpose. According to the microscopic reversibility principle, the path followed by the entering and leaving water molecules must be equivalent. In this sense, and using the simple transition-state theory, the transition state can be located when the distances of the involved water molecules with respect to the metal ion are equal. Locating the value at which it happens, one can identify if both water molecules are in the first or second hydration shell regions, and consequently, establishing if the mechanism has an associative or dissociative character.[34] The limiting radius that separates both shells is the first minimum in the Ca–O RDF (3.45 Å). Figure 8 shows the histogram obtained following this approach. Also in Fig. 8 is included the histogram of the $O-Ca^{2+}-O$ angle at the instant in which the transition state is located. On the basis of the aforementioned criterion, 45% of the exchanges proceed via dissociative activation modes (I_D) and the remaining 55% via associative ones (I_A). However, it is clear that a large mechanistic variability is present, spanning the Ca–O distance range of the intermediate states in ~3 Å. This large variability is understood more clearly if specific trajectories are observed. In Fig. 9 some examples of the exchanges observed are considered. The time evolution of the Ca–O distances for the waters involved and the corresponding coordination number obtained for that period are shown. The first case clearly shows an (almost) instantaneous interchange of dissociative character (I_D), in which the coordination number decreases temporarily during the exchange process. An interchange of associative character (I_A) showing a transition state with a finite lifetime is shown in part b. The process is accompanied by a temporary increase of the coordination number. In both cases we can assume that the structure involved in the transition state presents nine water molecules: n_c+2 for I_D and n_c for I_A. However, together with these well resolved mechanisms more complex situations are found as well. As an example, in Fig. 9(c) a mechanism involving three water molecules is considered. Although the entering and leaving solvent molecules equal their Ca–O distances at 4.94 Å, the coordination number at that instant is eight, and not seven as could be expected for a dissociative interchange where just these two molecules are

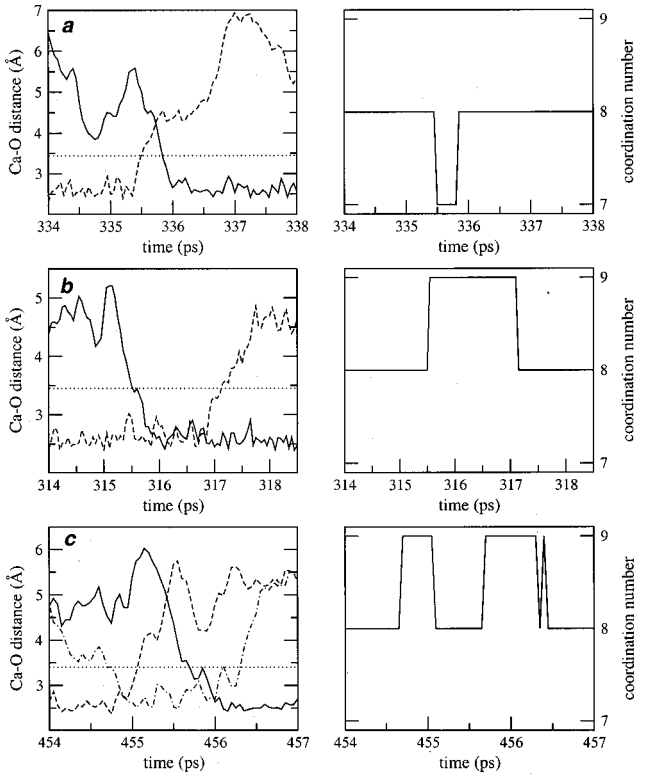

FIG. 9. Evolution of the calcium–oxygen distance for the water molecules involved in three mechanistically different exchange events in simulation A. Right-hand side graphs show the evolution of the coordination number for the same period. Dotted horizontal line marks the limit differentiating the first and second hydration shells (3.45 Å).

involved in the exchange process. The reason is the transient presence of a third water molecule in the first hydration region while the exchange is taking place. Different from the other two cases, in this example the structure of the transition state contains ten solvent molecules. However, following the aforementioned geometrical definition, the mechanism is clearly dissociative. This is just an example of the large variability that can be found in the most *simple* situation: water–water exchange.

When ammonia is introduced in the solution, the situation becomes more complex for two reasons. On the one hand, the possible exchange events different in nature increase. As long as the ammonia presence increases, the probability of finding a water–water exchange is reduced and exchanges involving ammonia molecules take place (Table VII). Even more, for the mixed situations (exchanges involving water and ammonia), there is no clear definition of the cutoff radius that defines the limit between the first and second shells: Ca–O and Ca–N RDFs present the first minimum at different distances.

TABLE VII. Percentages of the different first–second shell solvent exchanges.

Simulation	Water–water	Water–ammonia	Ammonia–ammonia
B	92%	8%	...
C	20%	52%	28%
D	6%	25%	69%

On the other hand, the displacement of the coordination number from eight to nine, provokes the appearance of elimination and addition reactions, in which structures with eight and nine solvent molecules are alternated, not allowing the identification of the pair of solvent molecules that exchange their solvation shells. Nonetheless, when possible, the coupled pairs were identified, which can yield interesting information about the most common exchange events present in the neighborhood of the ion when more that one solvent is present. Table VII collects the percentage of the different solvent exchanges found in simulations B, C, and D. There is a clear and progressive decrease in the number of water–water exchanges while the opposite tendency is observed for those implying two ammonia molecules. Mixed exchanges reach a maximum in simulation C. In fact, these types of exchanges are the ones that allow changes in the chemical composition of the solvated ion. Therefore it is in this simulation where a larger chemical variety of structures could be expected, as confirmed by the distributions.[41] Obviously, the probability of finding a given type of exchange depends on the number of molecules of each type present in the first and second shells. In this sense, the tendencies observed agree with the evolution of the number of water and ammonia molecules in the first solvation shell (Table II). However, the lowest water/ammonia ratio in the second shell is >3. In this sense, both solvents are not equivalent, and ammonia has a much greater propensity to participate in solvent exchanges than water, at least in the conditions the simulations were performed. These findings are in agreement with the previously computed MRTs (Table V).

IV. CONCLUSIONS

Dilute ammonia aqueous solutions in the presence of calcium ion have been studied by means of MD simulations using the effective interaction potentials previously developed.[25] The use of these potentials in cluster computations provided structural tendencies that are now confirmed by the subsequent simulations. The evolution of the solvation properties of calcium ion with solvent composition have been studied providing very detailed information at a structural and dynamical level of the solvation phenomenon of Ca^{2+}. A preferential solvation by ammonia has been observed, even at very low concentrations. The substitution of waters in the first hydration shell by ammonia molecules, clearly changes the structure of the solvated ion, and a tendency to accommodate a larger number of solvent molecules in the nearest neighborhood of the ion is observed. This increase in the solvation number, however, is accompanied by an increase in the intrinsic lability of the new representative structures, as shown by the mean lifetimes of the complexes with different sizes. Solvent–solvent interactions, particularly hydrogen bonding, are revealed as a key point to understanding the observed tendencies. In this sense, the response of ammonia to the ion field is larger than that of water, which is observed both at structural (tilt angle) and dynamical levels (reorientational times). The study of the solvent exchange phenomenon around the metal ion yields a large variety of exchange mechanisms, with ammonia molecules, when present, having a greater propensity to participate in the exchanges.

MD results presented here have shown a good performance for the potentials developed in the PCM framework, motivating similar strategies for more complicated situations.

ACKNOWLEDGMENTS

Dr. K. Refson is thanked for supplying the modified version of the MOLDY code and Professor A. Tani for helpful discussions. J.M.M. thanks the Ministerio de Educación y Cultura (M.E.C.) of Spain for a postdoctoral fellowship.

[1] J. J. R. Fraústo da Silva and R. J. P. Williams, *The Biological Chemistry of the Elements* (Oxford University Press, Oxford, 1996).
[2] R. J. P. Williams and J. J. R. Fraústo da Silva, Coord. Chem. Rev. **200–202**, 247 (2000).
[3] W. Kaim and B. Schwederski, *Bioinorganic Chemistry* (Wiley, Chichester, 1994).
[4] M. M. Probst, T. Radnai, K. Heinzinger, P. Bopp, and B. M. Rode, J. Phys. Chem. **89**, 753 (1985).
[5] D. G. Bounds, Mol. Phys. **6**, 1335 (1985).
[6] G. Pálinkás and K. Heinzinger, Chem. Phys. Lett. **126**, 251 (1986).
[7] S. Obst and H. Bradaczek, J. Phys. Chem. **100**, 15677 (1996).
[8] J. Aqvist, J. Phys. Chem. **94**, 8021 (1990).
[9] F. M. Floris, M. Persico, A. Tani, and J. Tomasi, Chem. Phys. Lett. **227**, 126 (1994).
[10] M. I. Bernal-Uruchurtu and I. Ortega-Blake, J. Chem. Phys. **103**, 1588 (1995).
[11] S. G. Kalko, G. Sesé, and J. A. Padró, J. Chem. Phys. **104**, 9578 (1996).
[12] X. Periole, D. Allouche, J. P. Daudey, and Y. H. Sanejouand, J. Phys. Chem. B **101**, 5018 (1997).
[13] A. Tongraar, K. R. Liedl, and B. M. Rode, J. Phys. Chem. A **101**, 6299 (1997).
[14] X. Periole, D. Allouche, A. Ramírez-Solís, I. Ortega-Blake, J. P. Daudey, and Y. H. Sanejouand, J. Phys. Chem. B **102**, 8579 (1998).
[15] S. Koneshan, J. C. Rasaiah, R. M. Lynden-Bell, and S. H. Lee, J. Phys. Chem. B **102**, 4193 (1998).
[16] H.-S. Kim, Chem. Phys. **257**, 183 (2000).
[17] F. Jalilehvand, D. Spangberg, P. Lindqvist-Reis, K. Hermansson, I. Persson, and M. Sandstrom, J. Am. Chem. Soc. **123**, 431 (2001).
[18] E. Guardia, G. Sesé, J. A. Padró, and S. G. Kalko, J. Sol. Chem. **28**, 1113 (1999).
[19] M. Kaupp and P. v. R. Schleyer, J. Phys. Chem. **96**, 7316 (1992).
[20] E. Magnusson, J. Phys. Chem. **98**, 12558 (1994).
[21] T. Kerdcharoen and S. Hannongbua, Chem. Phys. Lett. **310**, 333 (1999).
[22] M. Alcamí, A. I. González, O. Mó, and M. Yánez, Chem. Phys. Lett. **307**, 244 (1999).
[23] S. Petrie and L. Radom, Int. J. Mass Spectrom **192**, 173 (1999).
[24] W. Sidhisoradej, S. Hannongbua, and D. Ruffolo, Z. Naturforsch., A: Phys. Sci. **53**, 208 (1998).
[25] F. M. Floris, José Martinez, and J. Tomasi, J. Chem. Phys. **116**, 5448 (2002), preceding paper.
[26] H. J. C. Berendsen, J. R. Grigera, and T. P. Straatsma, J. Phys. Chem. **91**, 6269 (1987).
[27] R. C. Rizzo and W. L. Jorgensen, J. Am. Chem. Soc. **121**, 4827 (1999).
[28] K. Refson, Comput. Phys. Commun. **126**, 310 (2000).
[29] H. Goldstein, 2nd ed., Classical Mechanics (Addison–Wesley, Reading, 1980).
[30] M. P. Allen and D. J. Tildesley, *Computer Simulations of Liquids* (Oxford University Press, Oxford, 1987).
[31] T. Yamaguchi, S. Hayashi, and H. Ohtaki, Inorg. Chem. **28**, 2434 (1989).
[32] L. Licheri, G. Piccaluga, and G. Pinna, J. Chem. Phys. **63**, 4412 (1975).
[33] N. A. Hewish, G. W. Neilson, and J. E. Enderby, Nature (London) **297**, 138 (1982).
[34] H. Ohtaki and T. Radnai, Chem. Rev. **93**, 1157 (1993).
[35] M. Magini, G. Licheri, G. Paschina, G. Piccaluga, and G. Pinna, *X-Ray Diffraction of Ions in Aqueous Solutions: Hydration and Complex Formation* (CRC Press, Boca Raton, FL, 1988).

[36] J. M. Martínez, R. R. Pappalardo, and E. Sánchez Marcos, J. Am. Chem. Soc. **121**, 3175 (1999).
[37] J. M. Martínez, R. R. Pappalardo, and E. Sánchez Marcos, J. Chem. Phys. **110**, 1669 (1999).
[38] F. M. Floris, M. Persico, A. Tani, and J. Tomasi, Chem. Phys. **195**, 207 (1995).
[39] H. Kanno, J. Phys. Chem. **92**, 4232 (1988).
[40] D. E. Irish and M. H. Brooker, *Advances in Infrared and Raman Spectroscopies* (Heyden, London, 1976), Vol. 2, Chap. 6.
[41] See EPAPS Document No. E-JCPSA6-116-306213 for supplementary figures. This document may be retrieved via the EPAPS homepage (http://www.aip.org/pubservs/epaps.html) or from ftp.aip.org in the directory /epaps/. See the EPAPS homepage for more information.
[42] D. Marx, J. Hutter, and M. Parrinello, Chem. Phys. Lett. **241**, 457 (1995).
[43] J. M. Martínez, R. R. Pappalardo, and E. Sánchez Marcos, J. Chem. Phys. **109**, 1445 (1998).
[44] V. I. Chizhik, Mol. Phys. **90**, 653 (1997).
[45] R. W. Impey, P. A. Madden, and I. R. McDonald, J. Phys. Chem. **87**, 5071 (1983).
[46] A. E. Garcia and L. Stiller, J. Comput. Chem. **14**, 1396 (1993).
[47] S. F. Lincoln and A. E. Merbach, Adv. Inorg. Chem. **42**, 1 (1995).
[48] T. Kowall, F. Foglia, L. Helm, and A. E. Merbach, J. Am. Chem. Soc. **117**, 3790 (1995).
[49] T. Kowall, F. Foglia, L. Helm, and A. E. Merbach, Chem. Eur. J. **2**, 285 (1996).
[50] L. Helm and A. E. Merbach, Coord. Chem. Rev. **187**, 151 (1999).
[51] R. van Eldik, Coord. Chem. Rev. **182**, 373 (1999).